

Superconductivity and Structural Phase Transitions in Caged Compounds RT_2Zn_{20} ($R = La, Pr, T = Ru, Ir$)

Takahiro ONIMARU^{1*}, Keisuke T. MATSUMOTO¹, Yukihiro F. INOUE¹, Kazunori UMEO²,
Yuta SAIGA³, Yoshitaka MATSUSHITA⁴, Ryuji TAMURA⁵, Kazue NISHIMOTO⁵,
Isao ISHII¹, Takashi SUZUKI¹, and Toshiro TAKABATAKE^{1,3}

¹Department of Quantum Matter, Graduate School of Advanced Sciences of Matter, Hiroshima University,
Higashihiroshima, Hiroshima 739-8530, Japan

²Cryogenics and Instrumental Analysis Division, N-BARD, Hiroshima University,
Higashihiroshima, Hiroshima 739-8526, Japan

³Institute for Advanced Materials Research, Hiroshima University, Higashihiroshima, Hiroshima 739-8530, Japan

⁴NIMS Beamline Station at SPring-8, National Institute for Materials Science, Sayo, Hyogo 679-5148, Japan

⁵Department of Materials Science and Technology, Tokyo University of Science, Noda, Chiba 278-8510, Japan

(Received December 24, 2009; accepted January 6, 2010; published February 25, 2010)

Electrical resistivity ρ , specific heat C , magnetization M measurements are reported on four compounds, $LaRu_2Zn_{20}$, $PrRu_2Zn_{20}$, $LaIr_2Zn_{20}$, and $PrIr_2Zn_{20}$, which crystallize in a cubic $CeCr_2Al_{20}$ -type structure. $LaRu_2Zn_{20}$, $LaIr_2Zn_{20}$, and $PrIr_2Zn_{20}$ show superconducting transitions at $T_C = 0.2, 0.6$, and ~ 0.05 K, respectively, whereas $PrRu_2Zn_{20}$ remains a normal state down to 0.04 K. This is the first observation of superconductivity in the family of RT_2X_{20} ($T =$ transition metal; $X = Al$ and Zn). Furthermore, structural phase transitions manifest themselves at $T_s = 150, 138$, and 200 K for $LaRu_2Zn_{20}$, $PrRu_2Zn_{20}$, and $LaIr_2Zn_{20}$, respectively. No magnetic transition is found in $PrRu_2Zn_{20}$ and $PrIr_2Zn_{20}$ down to 1.8 K. On cooling $PrIr_2Zn_{20}$ below 2 K, the specific heat divided by temperature, C/T , continuously increases and reaches $5 J/(K^2 \cdot mol)$ at 0.4 K, suggesting that $Pr 4f^2$ electrons are involved in the heavy-fermion state, as observed in a related compound $YbCo_2Zn_{20}$.

KEYWORDS: RT_2Zn_{20} , caged structure, superconductivity, structural phase transition
DOI: [10.1143/JPSJ.79.033704](https://doi.org/10.1143/JPSJ.79.033704)

The interest in strongly correlated electron systems with caged structures has been stimulated by the observations of attractive phenomena, such as heavy-fermion state, superconductivity, multipole ordering, and rattling of guest atoms. An example is the family of rare-earth-filled skutterudites RT_4X_{12} , where rare-earth (R) guest atoms are encapsulated in highly symmetric cages with a relatively large space for R^{3+} ions. In particular, the compounds with $R = Pr$ and Sm show various interesting phenomena, such as heavy-fermion superconductivity in $PrOs_4Sb_{12}$,¹⁾ scalar-type multipole ordering in $PrFe_4P_{12}$, metal-insulator transition in $PrRu_4P_{12}$, and a heavy-fermion state attributed to the rattling motion of the guest atoms in $SmOs_4Sb_{12}$.²⁾

Another class of caged compounds RT_2X_{20} ($X = Al$ and Zn) have the cubic $CeCr_2Al_{20}$ -type structure with the space group $Fd\bar{3}m$ and $Z = 8$,³⁾ where the R atoms are encapsulated in the Frank-Kasper cages formed by 16 zinc atoms. Yb -based compounds YbT_2Zn_{20} ($T = Fe, Co, Ru, Rh, Os$, and Ir) show heavy-fermion behavior; in particular, $YbCo_2Zn_{20}$ has the largest electronic specific heat coefficient of $\gamma = 8 J/(K^2 \cdot mol)$.⁴⁾ Furthermore, applying pressures above 1 GPa induces a magnetic transition at $T_M \sim 0.15$ K. Therefore, $YbCo_2Zn_{20}$ is considered to be located in the vicinity of a quantum critical point.⁵⁾ Ultrasonic measurements on $YbCo_2Zn_{20}$ revealed the highly degenerated low-lying levels of the $4f$ electrons of Yb ions under a weak crystalline electric field (CEF).⁶⁾ Recently, the dHvA effect measurements on $YbIr_2Zn_{20}$ have revealed large cyclotron masses of $4-27m_0$, to which the $4f$ electrons contribute.⁷⁾ As is shown above, the magnetic and transport properties of the

RT_2X_{20} ($X = Zn, Al$) have been intensively studied, however, no superconductivity has been observed.

In the present work, we focus on RT_2Zn_{20} ($R = La$ and Pr ; $T = Ru$ and Ir), where non-Kramers Pr ions or non-magnetic La ions reside in the cages. In PrT_2Zn_{20} , multipole phase transitions and strong hybridizations between $4f$ electrons and conduction bands are expected to occur owing to the highly degenerate ground state. We have performed electrical resistivity ρ , specific heat C , magnetization M , thermopower S , and ultrasonic measurements on single-crystalline samples. Thereby, structural phase transitions were found to occur above 100 K. The measurements of ρ , C , and AC magnetic susceptibility revealed superconductivity below 1 K, which is the first observation of superconductivity in the family of RT_2X_{20} ($X = Al$ and Zn).

Single-crystalline samples were prepared by the self-flux method described in the previous paper.⁵⁾ The samples were characterized by the X-ray powder diffraction technique, electron-probe microanalysis (EPMA), and transmission electron microscopic method (TEM). The crystal compositions determined by averaging over 10 different regions for each crystal with a JEOL JXA-8200 analyzer are $PrRu_{1.96(3)}Zn_{20.30(11)}$ and $PrIr_{1.91(2)}Zn_{20.16(13)}$, where it was assumed that the Pr sites are fully occupied. Impurity phases of binary $RuZn_9$, $IrZn_{6.5}$, and $IrZn_{8.5}$ alloys were detected in the samples of RRu_2Zn_{20} and RIr_2Zn_{20} , respectively. Their volume fractions are less than 5% in view of the back-scattering electron images. Furthermore, our specific heat measurements of the binary compounds confirmed that neither show phase transition down to 0.4 K. Powder X-ray diffraction measurements were performed in the temperature range from 300 to 3 K with $Cu K\alpha$ radiation. The structural

*E-mail: onimaru@hiroshima-u.ac.jp

Table I. Lattice parameters, structural phase transition temperatures T_s , superconducting transition temperatures T_C , magnetic transition temperatures T_M , and CEF ground state of $\text{LaRu}_2\text{Zn}_{20}$, $\text{PrRu}_2\text{Zn}_{20}$, $\text{LaIr}_2\text{Zn}_{20}$, and $\text{PrIr}_2\text{Zn}_{20}$.

Compounds	Lattice parameter (Å)	Structural phase transition T_s (K)	Superconducting transition T_C (K)	Magnetic or multipolar transition T_M (K)	CEF ground state of the Pr ion
$\text{LaRu}_2\text{Zn}_{20}$	14.4263(2)	150	0.2	—	—
$\text{PrRu}_2\text{Zn}_{20}$	14.3467(4)	138	—	none	singlet ($T < T_s$)
$\text{LaIr}_2\text{Zn}_{20}$	14.3535(2)	200	0.6	—	—
$\text{PrIr}_2\text{Zn}_{20}$	14.2729(2)	—	~ 0.05	$< 0.4?$	doublet?

parameters were refined by single-crystal X-ray diffraction analysis at 293 K with Mo $K\alpha$ radiation using a Bruker SMART APEX CCD area-detector diffractometer. The TEM observation was performed using JEM2010F equipped with a liquid N_2 stage operating at an acceleration voltage of 200 kV. Magnetization was measured using a commercial SQUID magnetometer (Quantum Design MPMS) between 1.8 and 350 K at magnetic fields up to 5 T. Electrical resistance was measured by a standard four-probe AC method in a laboratory-built system with a Gifford-McMahon-type refrigerator and a commercial Cambridge Magnetic Refrigeration mFridge mF-ADR50. Thermopower from 4 to 300 K was measured using a laboratory-made probe by applying a temperature difference of 0.04–0.3 K along a bar-shaped sample. Specific heat was measured by a relaxation method at temperatures between 0.4 and 300 K. AC magnetic susceptibility was measured down to 40 mK using a laboratory-made system installed in the mFridge mF-ADR50. Elastic constants were measured using the phase comparison-type pulse echo method.

In the ideal structure of $\text{RT}_2\text{Zn}_{20}$, the R atoms fully occupy the $8a$ site at T_d point symmetry, T at the $16d$ site, and Zn at the $96g$, $48f$, and $16c$ sites. Each R atom is encapsulated in the Frank–Kasper polyhedron formed by 16 zinc atoms at the $96g$ and $16c$ sites. Another structural aspect to be noted is that the T atoms form a pyrochlore lattice. The lattice parameter for $\text{PrRu}_2\text{Zn}_{20}$ was reported to be $14.336(1)$ Å.³⁾ To examine the structure, we performed X-ray diffraction experiments on single-crystalline samples of $\text{PrRu}_2\text{Zn}_{20}$ and $\text{PrIr}_2\text{Zn}_{20}$. The crystal structure of $\text{PrIr}_2\text{Zn}_{20}$ was confirmed to be the same as reported. For $\text{PrRu}_2\text{Zn}_{20}$, however, the fourth Zn site of $192i$ was necessary to reproduce the data. The occupancies of the Zn sites of $96g$, $48f$, and $192i$ are less than 1, indicating that the Frank–Kasper cage is slightly distorted. The lattice parameters were determined to be $14.3467(4)$ Å for $\text{PrRu}_2\text{Zn}_{20}$ and $14.2729(2)$ Å for $\text{PrIr}_2\text{Zn}_{20}$ as shown in Table I. The results of a detailed analysis of the crystal structure will be reported elsewhere.

Figure 1 shows the temperature dependence of the electrical resistivity ρ . The data below 10 K are represented in the lower inset in Fig. 1. On cooling below 1 K, ρ drops to zero at 0.2 K for $\text{LaRu}_2\text{Zn}_{20}$, 0.6 K for $\text{LaIr}_2\text{Zn}_{20}$, and 0.05 K for $\text{PrIr}_2\text{Zn}_{20}$. The AC magnetic susceptibility χ_{AC} was measured to estimate the superconducting volume fraction in the samples by comparing the diamagnetic signal with that of the reference Sn sample of almost the same shape. Figure 2 shows the rapid drops in $\chi_{AC}(T)$ at $T_C = 0.2$, 0.6, and 0.05 K for $\text{LaRu}_2\text{Zn}_{20}$, $\text{LaIr}_2\text{Zn}_{20}$, and $\text{PrIr}_2\text{Zn}_{20}$,

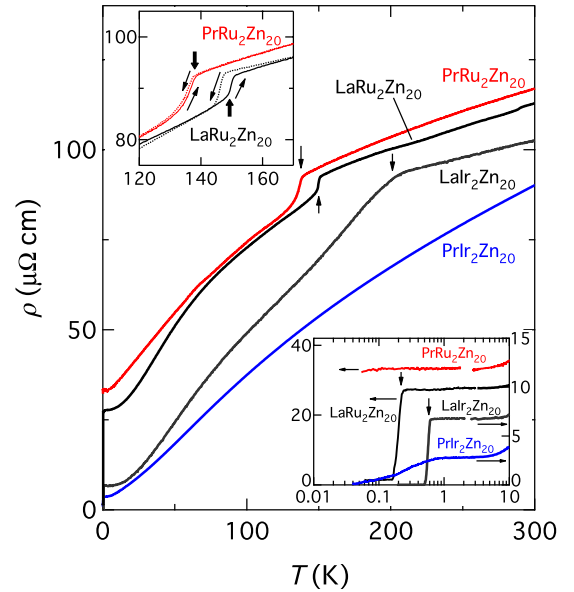


Fig. 1. (Color online) Temperature dependence of the electrical resistivity ρ of $\text{LaRu}_2\text{Zn}_{20}$, $\text{PrRu}_2\text{Zn}_{20}$, $\text{LaIr}_2\text{Zn}_{20}$, and $\text{PrIr}_2\text{Zn}_{20}$. For $\text{LaRu}_2\text{Zn}_{20}$ and $\text{PrRu}_2\text{Zn}_{20}$, $\rho(T)$ jumps at $T_s = 150$ and 138 K, respectively. As indicated in the upper inset, $\rho(T)$ shows hysteresis, indicating that the transitions are of first order. For $\text{LaIr}_2\text{Zn}_{20}$, $\rho(T)$ bends at $T_s = 200$ K. On cooling below 1 K, ρ drops to zero at 0.2, 0.6, and ~ 0.05 K for $\text{LaRu}_2\text{Zn}_{20}$, $\text{LaIr}_2\text{Zn}_{20}$, and $\text{PrIr}_2\text{Zn}_{20}$, respectively, as shown in the right-bottom inset.

respectively; $\chi_{AC}(T)$ remains constant in $\text{PrRu}_2\text{Zn}_{20}$ down to 0.04 K. These behaviors are very consistent with that of $\rho(T)$. Actually, the onset temperature of the drop in $\rho(T)$ for $\text{LaIr}_2\text{Zn}_{20}$ shown in Fig. 2 agrees with that of the drop in χ_{AC} . The drop in AC voltage for $\text{LaIr}_2\text{Zn}_{20}$ below T_C is almost the same as that for the reference Sn, indicating the bulk nature of the superconductivity. The bulk nature was confirmed by a clear jump in $C(T)$ at $T_C = 0.58$ K, as shown in the inset in Fig. 2. The electronic specific heat coefficient γ was estimated to be 14.4 mJ/(K²·mol) by extrapolating the C/T vs T^2 plot from the data above T_C to $T = 0$. $\Delta C/\gamma T_C = 0.53$ evaluated in the present sample is smaller than $\Delta C/\gamma T_C = 1.43$ expected for a BCS superconductor. This seems to be inconsistent with the fact that the diamagnetic signal in χ_{AC} almost agrees with that of the BCS superconductor Sn reference. However, the reduction in the volume fraction evaluated in the $C(T)$ measurement probably results from a residual magnetic field in the superconducting magnet used in the present $C(T)$ measurements. Actually, T_C is slightly lower in the C measurement than in

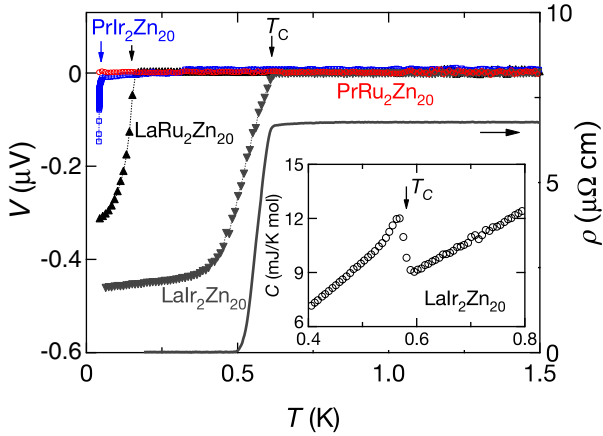


Fig. 2. (Color online) Temperature dependence of the AC magnetic susceptibility of $\text{LaRu}_2\text{Zn}_{20}$, $\text{PrRu}_2\text{Zn}_{20}$, $\text{LaIr}_2\text{Zn}_{20}$, and $\text{PrIr}_2\text{Zn}_{20}$, where the paramagnetic contributions were eliminated for clarity. On cooling, χ_{AC} values suddenly drop at 0.2, 0.6, and 0.05 K for $\text{LaRu}_2\text{Zn}_{20}$, $\text{LaIr}_2\text{Zn}_{20}$, and $\text{PrIr}_2\text{Zn}_{20}$, respectively, indicating a superconducting transition. The $\rho(T)$ of $\text{LaIr}_2\text{Zn}_{20}$ is also shown in the right-hand axis for comparison. The inset shows the $C(T)$ of $\text{LaIr}_2\text{Zn}_{20}$ in the vicinity of $T_C = 0.58$ K.

the ρ and χ_{AC} measurements. To the best of our knowledge, this is the first observation of superconductivity in the RT_2X_{20} family ($X = \text{Al}$ and Zn). It should be noted that the T_C of the Pr compound is lower than those of the La counterparts. Therefore, the $4f$ electrons of Pr ions may destabilize the superconductivity, as was found in rare-earth-based Chevrel phase superconductors.⁸⁾

Let us focus on the $\rho(T)$ data in the main frame in Fig. 1. For $\text{LaRu}_2\text{Zn}_{20}$ and $\text{PrRu}_2\text{Zn}_{20}$, $\rho(T)$ jumps at $T_s = 150$ and 138 K, respectively. The temperature dependence shows hysteresis, as shown in the upper inset, indicating that the transitions are of first order. For $\text{LaIr}_2\text{Zn}_{20}$, $\rho(T)$ bends at $T_s = 200$ K, although for $\text{PrIr}_2\text{Zn}_{20}$, no anomaly appears up to 300 K. The thermopower of $\text{PrRu}_2\text{Zn}_{20}$ also shows a clear minimum at around T_s (not presented here). Figure 3 shows corresponding anomalies in the specific heat of $\text{LaRu}_2\text{Zn}_{20}$, $\text{PrRu}_2\text{Zn}_{20}$, and $\text{LaIr}_2\text{Zn}_{20}$ at 150, 138, and 200 K, respectively. The peaks at T_s in $\text{LaRu}_2\text{Zn}_{20}$ and $\text{PrRu}_2\text{Zn}_{20}$ are rather sharp and are accompanied by hysteresis, which is the hallmark of the first-order transition. In the magnetic susceptibility $\chi = M/B$ of $\text{LaRu}_2\text{Zn}_{20}$ in $B = 5$ T, a cusp appears at T_s , as shown in the inset in Fig. 4, suggesting a decrease in the electronic density of states below T_s . The TEM examination below T_s revealed superlattice reflections in both $\text{LaRu}_2\text{Zn}_{20}$ and $\text{PrRu}_2\text{Zn}_{20}$. This observation indicates that the crystal lattice is modulated at T_s . The results of TEM will be reported in detail elsewhere. On the other hand, the $C(T)$ of $\text{LaIr}_2\text{Zn}_{20}$ shows a broad peak at 200 K, which coincides with the bend in $\rho(T)$. Both observations suggest the transition in $\text{LaIr}_2\text{Zn}_{20}$ to be of second order.

We recall here that in the pyrochlore compound $\text{Cd}_2\text{Re}_2\text{O}_7$, the superconductivity below 1.0 K coexists with structural phase transitions at $T_{s1} = 200$ K and $T_{s2} = 120$ K.^{9,10)} The structural phase transitions were attributed to the lattice instability induced by highly degenerated hole bands near the Fermi level.¹¹⁾ By applying a high pressure above a critical pressure of 3.5 GPa, the superconductivity disappeared and T_{s1} dropped to $T = 0$. These results strongly

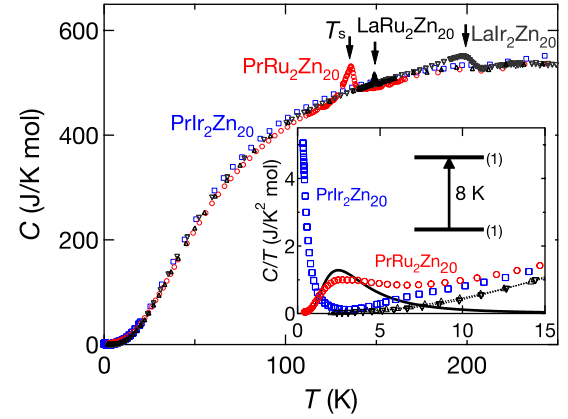


Fig. 3. (Color online) Temperature dependence of the specific heat of $\text{LaRu}_2\text{Zn}_{20}$ (upward triangle), $\text{PrRu}_2\text{Zn}_{20}$ (circle), $\text{LaIr}_2\text{Zn}_{20}$ (downward triangle), and $\text{PrIr}_2\text{Zn}_{20}$ (square). In $\text{LaRu}_2\text{Zn}_{20}$ and $\text{PrRu}_2\text{Zn}_{20}$, sharp peaks appearing at $T_s = 150$ and 138 K, respectively, indicate first order phase transitions. In $\text{LaIr}_2\text{Zn}_{20}$, a broad peak appears at $T_s = 200$ K, whereas no anomaly appears in $\text{PrIr}_2\text{Zn}_{20}$ up to 300 K. The inset shows the temperature dependence of C/T . In $\text{PrRu}_2\text{Zn}_{20}$, a Schottky-like anomaly appears at approximately 2.5 K. The black bold curve is obtained using a singlet-singlet two-level model with $\Delta E = 8$ K. In $\text{PrIr}_2\text{Zn}_{20}$, C/T decreases on cooling down to 3 K, increases and reaches ~ 5 J/(K²·mol) at 0.4 K.

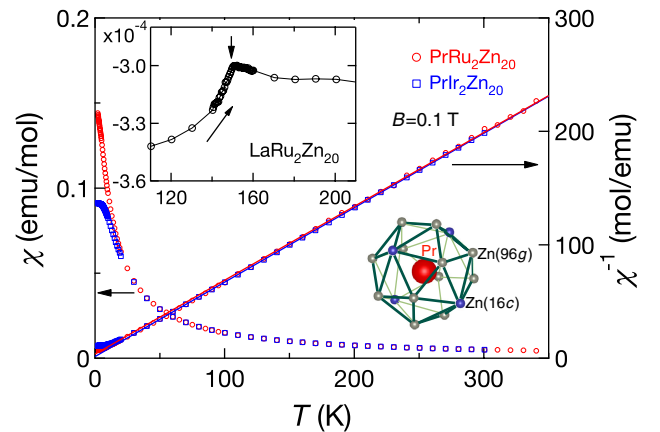


Fig. 4. (Color online) Temperature dependence of the magnetic susceptibility χ and the inverse χ^{-1} for $\text{PrRu}_2\text{Zn}_{20}$ (circle) and $\text{PrIr}_2\text{Zn}_{20}$ (square) at a magnetic field of $B = 0.1$ T. Above 30 K, $\chi(T)$ follows the Curie-Weiss law with the effective magnetic moment of the trivalent Pr ion. The inset shows the cusp in $\chi(T)$ at $T_s = 150$ K for $\text{LaRu}_2\text{Zn}_{20}$. The right-hand inset shows a Pr atom encapsulated in a Frank-Kasper polyhedron composed of sixteen Zn atoms at the 16c and 96g sites.

suggested the relationship between the superconductivity and the structural phase transitions.¹²⁾

We next focus on the magnetic properties of the Pr ions in $\text{PrRu}_2\text{Zn}_{20}$ and $\text{PrIr}_2\text{Zn}_{20}$. As is shown in Fig. 4, $\chi(T)$ values for $30 < T < 350$ K obey the Curie-Weiss law, with the effective magnetic moments of 3.50(2) and 3.49(2) μ_B/Pr^{3+} , and the paramagnetic Curie temperatures θ_p of -5.6 and -2.3 K, respectively. This indicates that the intersite magnetic interactions between the trivalent Pr ions are antiferromagnetic but very weak. The $\chi(T)$ of $\text{PrRu}_2\text{Zn}_{20}$ continuously increases with decreasing temperature down to 2 K, indicating a paramagnetic ground state with a high degeneracy or small CEF level splitting. The elastic constant

of $\text{PrRu}_2\text{Zn}_{20}$ softens on cooling from 300 K and exhibits a broad minimum at $T_s = 138$ K, which is followed by continuous hardening. This indicates that a quadrupolar degree of freedom is eliminated at T_s by breaking the cubic symmetry at the Pr site. Thereby, a nonmagnetic singlet state can be formed below T_s . The formation of the singlet ground state in $\text{PrRu}_2\text{Zn}_{20}$ is supported by the appearance of a Schottky peak at 2.5 K in C/T , as shown in the inset in Fig. 3. The peak in C/T is reproduced by a model of singlet–singlet two levels separated by 8 K. The electronic specific heat coefficient γ was estimated to be 6.4 and 22 $\text{mJ}/(\text{K}^2\cdot\text{mol})$ for $\text{LaRu}_2\text{Zn}_{20}$ and $\text{PrRu}_2\text{Zn}_{20}$, respectively. On the other hand, the $\chi(T)$ of $\text{PrIr}_2\text{Zn}_{20}$ approaches a constant value at temperatures below 10 K, indicating the CEF ground state to be a Van-Vleck paramagnetic state. In fact, the C/T of $\text{PrIr}_2\text{Zn}_{20}$ increases on cooling and reaches $5 \text{ J}/(\text{K}^2\cdot\text{mol})$ at 0.4 K. The results of $\chi(T)$ and $C(T)$ suggest the CEF ground state to be degenerated. What remains to be studied is how the superconductivity at 0.05 K is affected by the multipolar degrees of freedom in the state.

In summary, we have found superconductivity in the family of $\text{RT}_2\text{Zn}_{20}$ at $T_C = 0.2, 0.6,$ and ~ 0.05 K for $\text{LaRu}_2\text{Zn}_{20}$, $\text{LaIr}_2\text{Zn}_{20}$, and $\text{PrIr}_2\text{Zn}_{20}$, respectively. Furthermore, structural phase transitions appear at much higher temperatures of $T_s = 150, 138,$ and 200 K for $\text{LaRu}_2\text{Zn}_{20}$, $\text{PrRu}_2\text{Zn}_{20}$, and $\text{LaIr}_2\text{Zn}_{20}$, respectively, although no phase transition occurs up to 300 K in $\text{PrIr}_2\text{Zn}_{20}$. Below T_s , superlattice reflection was detected by the transmission electron diffraction method. The lattice parameters and the transition temperatures are summarized in Table I. $\text{PrRu}_2\text{Zn}_{20}$ and $\text{PrIr}_2\text{Zn}_{20}$ show paramagnetic behavior down to 1.8 K. The CEF ground state of the former is a nonmagnetic singlet, while that of the latter is probably degenerated. The magnetic or multipolar transition T_M and the CEF ground states are also summarized in Table I. For $\text{PrIr}_2\text{Zn}_{20}$, C/T increases up to $5 \text{ J}/(\text{K}^2\cdot\text{mol})$ on cooling at 0.4 K, suggesting a heavy-fermion state, as observed in a related compound $\text{YbCo}_2\text{Zn}_{20}$. The interplay between the superconductivity and structural phase transition should be further studied.

Acknowledgments

The authors would like to thank Z. Hiroi, F. Iga, and Y. Muro for helpful discussions. We also thank Y. Shibata for the electron-probe microanalysis performed at N-BARD, Hiroshima University. The electrical resistivity, magnetization, specific heat, and low-temperature powder X-ray diffraction measurements were carried out at N-BARD, Hiroshima University. This work was financially supported by Grants-in-Aid from the Ministry of Education, Culture, Sports, Science and Technology of Japan, Nos. 18204032, 19051011, 20102004, and 21102516, and by The Mazda Foundation Research Grant, Japan.

- 1) E. D. Bauer, N. A. Frederick, P.-C. Ho, V. S. Zapf, and M. B. Maple: *Phys. Rev. B* **65** (2002) 100506.
- 2) See, for example, *J. Phys. Soc. Jpn.* **77** (2008) Suppl. A, and references therein.
- 3) T. Nasch, W. Jeitschko, and U. C. Rodewald: *Z. Naturforsch. B* **52** (1997) 1023.
- 4) M. S. Torikachvili, S. Jia, E. D. Mun, S. T. Hannahs, R. C. Black, W. K. Neils, D. Martien, S. L. Bud'ko, and P. C. Canfield: *Proc. Natl. Acad. Sci. U.S.A.* **104** (2007) 9960.
- 5) Y. Saiga, K. Matsubayashi, T. Fujiwara, M. Kosaka, S. Katano, M. Hedo, T. Matsumoto, and Y. Uwatoko: *J. Phys. Soc. Jpn.* **77** (2008) 053710.
- 6) Y. Nakanishi, T. Fujino, K. Ito, M. Nakamura, and M. Yoshizawa: *Phys. Rev. B* **80** (2009) 184418.
- 7) S. Yoshiuchi, M. Toda, M. Matsushita, S. Yasui, Y. Hirose, M. Ohta, K. Katayama, F. Honda, K. Sugiyama, M. Hagiwara, K. Kindo, T. Takeuchi, E. Yamamoto, Y. Haga, R. Settai, T. Tanaka, Y. Kubo, and Y. Ōnuki: *J. Phys. Soc. Jpn.* **78** (2009) 123711.
- 8) *Superconductivity in Ternary Compounds I, II*, ed. M. B. Maple and Ø. Fischer (Springer, Berlin, 1982).
- 9) Z. Hiroi, J. Yamaura, Y. Muraoka, and M. Hanawa: *J. Phys. Soc. Jpn.* **71** (2002) 1634.
- 10) M. Hanawa, Y. Muraoka, T. Tayama, T. Sakakibara, J. Yamaura, and Z. Hiroi: *Phys. Rev. Lett.* **87** (2001) 187001.
- 11) Z. Hiroi, M. Hanawa, Y. Muraoka, and H. Harima: *J. Phys. Soc. Jpn.* **72** (2003) 21.
- 12) Z. Hiroi, T. Yamauchi, T. Yamada, M. Hanawa, Y. Ohishi, O. Shimomura, M. Abliz, M. Hedo, and Y. Uwatoko: *J. Phys. Soc. Jpn.* **71** (2002) 1553.